

1

2 **The Aerosol Module in the Community Radiative Transfer Model** 3 **(v2.2 and v2.3): accounting for aerosol transmittance effects on the** 4 **radiance observation operator**

5 Cheng-Hsuan (Sarah) Lu^{1,2}, Quanhua Liu³, Shih-Wei Wei^{1,2}, Benjamin T. Johnson⁴, Cheng Dang¹,
6 Patrick G. Stegmann⁴, Dustin Grogan², Guoqing Ge^{5,6}, Ming Hu⁶, and Michael Lueken^{7,8}

7
8 ¹Joint Center for Satellite Data Assimilation, Boulder, CO, USA

9 ²Atmospheric Sciences Research Center, University at Albany, Albany, NY, USA

10 ³Center for Satellite Applications and Research, NOAA/NESDIS, College Park, MD, USA

11 ⁴Joint Center for Satellite Data Assimilation, College Park, MD, USA

12 ⁵Cooperative Institute for Research in Environmental Sciences, CU Boulder, CO, USA

13 ⁶Global System Laboratory, NOAA, Boulder, CO, USA

14 ⁷I.M. Systems Group, Inc., Rockville, MD, USA

15 ⁸Environmental Modeling Center, NOAA/NWS/NCEP, College Park, MD, USA

16
17 *Correspondence to:* Cheng-Hsuan Lu (clu@ucar.edu; clu4@albany.edu)

18 **Abstract**

19 The Community Radiative Transfer Model (CRTM), a sensor-based radiative transfer model, has been used within the
20 Gridpoint Statistical Interpolation (GSI) system for directly assimilating radiances from infrared and microwave sensors. We
21 conducted numerical experiments to illustrate how including aerosol radiative effects in CRTM calculations changes the GSI
22 analysis. Compared to the default aerosol-blind calculations, the aerosol influences reduced simulated brightness temperature
23 (BT) in thermal window channels, particularly over dust-dominant regions. A case study is presented, which illustrates how
24 failing to correct for aerosol transmittance effects leads to errors in meteorological analyses that assimilate radiances from
25 satellite IR sensors. In particular, the case study shows that assimilating aerosol-affected BTs significantly affects analyzed
26 temperatures in the lower atmosphere across several regions of the globe. Consequently, a fully-cycled aerosol-aware
27 experiment improves 1-5 day forecasts of wind, temperature, and geopotential height in the tropical troposphere and Northern
28 Hemisphere stratosphere. Whilst both GSI and CRTM are well documented with online user guides, tutorials and code
29 repositories, this article is intended to provide a joined-up documentation for aerosol absorption and scattering calculations in
30 the CRTM and GSI. It also provides guidance for prospective users of the CRTM aerosol option and GSI aerosol-aware
31 radiance assimilation. Scientific aspects of aerosol-affected BT in atmospheric data assimilation are briefly discussed.

32 1 Introduction

33 An accurate and computationally efficient radiative transfer model is essential in radiance assimilation for supporting weather
34 prediction, physical retrievals for satellite environmental data records, and inter-comparison ~~between different~~ remote
35 sensing ~~instruments~~sensors. The Community Radiative Transfer Model (CRTM) is a ~~sensor-based~~ radiative transfer model
36 ~~used extensively within satellite and remote sensing systems~~ (Weng, 2007; Han et al., 2007). It was primarily designed for
37 computing satellite radiances and has been ~~widely~~ used within the Gridpoint Statistical Interpolation (GSI, Wu et al., 2002;
38 Kleist et al., 2009) system for directly assimilating radiances from infrared (IR) and microwave (MW) sensors. Specifically,
39 clear-sky radiance calculations are carried out within the CRTM given the atmospheric scattering and absorption profile,
40 surface emissivity and reflectivity, and source functions. For cloudy radiance simulations (Stegmann et al., 2018), vertical
41 profiles of hydrometeor variables (e.g., cloud liquid water path and ice water path) are also required. Note that ~~the~~ CRTM
42 ~~was~~ not designed to ~~enact composition-radiation interaction effects within~~ ~~describe~~ spectral longwave and shortwave
43 ~~broadband~~ radiative transfer ~~calculations infor~~ general circulation models ~~s~~applications. Instead, ~~the CRTM was~~ ~~it is~~ developed
44 to support ~~monochromatic~~ satellite radiance ~~data~~ assimilation ~~from longwave and microwave sensors~~, and ~~for~~ satellite retrieval
45 ~~algorithm~~ development.

46
47 Past studies have demonstrated that aerosols significantly impact the simulation of brightness temperature (BT) in the IR
48 channels. BT is “a descriptive measure of radiation in terms of the temperature of a hypothetical blackbody emitting an
49 identical amount of radiation at the same wavelength” (American Meteorological Society, 2012). A reduction in retrieved BT
50 of 2-4 K in the atmospheric window region due to a strong dust outbreak was reported during the Saharan Dust Experiment
51 (SHADE) campaign (Highwood et al., 2003). Pierangelo et al. (2004) and Peyridieu et al. (2009) showed that the dust cooling
52 effects may reach 3 K in tropical atmospheric conditions depending on the dust burden. Diaz et al. (2001) found that there is
53 a significant increase in the errors of sea surface temperature (SST) retrievals in the presence of enhanced aerosol loading in
54 the atmosphere. The dust effects on satellite derived SST are constrained by accounting for dust absorption (Weaver et al.,
55 2003), applying a dust correction scheme (Nalli and Stowe, 2002; Merchant et al., 2006), or removing dust-contaminated
56 observations (Divakarla et al., 2012).

57
58 The impact of aerosol-affected BTs on the meteorological analysis fields has also been investigated. Wei et al. (2021a) used
59 the Global Data Assimilation System (GDAS, ~~Kleist et al., 2009~~) to assess the aerosol impact on the ~~meteorological~~GDAS
60 analysis. To do this, two GDAS experiments were conducted: a control cycled experiment, where aerosol transmittance effects
61 are not considered, and an offline non-cycled experiment, where aerosol transmittance effects are considered in the BT
62 calculations. The offline experiment uses identical observations and first guesses as the control experiment and thus the
63 response of atmospheric analysis to aerosol-aware radiance calculations can be clearly demonstrated. The experimental setup
64 in Wei et al. (2021a) followed the methodology presented in Kim et al. (2018), which is based on the Goddard Earth Observing

65 System (GEOS)-atmospheric data assimilation system (ADAS). Note that GEOS-ADAS and GDAS both used GSI and
66 CRTM, although the version and configuration differed. The studies by Kim et al. (2018) and Wei et al. (2021a) reported that:
67 (i) a considerable cooling effect on simulated BT when aerosols are considered; (ii) including aerosol transmittance effects in
68 the BT calculation improves the fit to observations over the dust-laden regions, and (iii) the offline aerosol-aware experiment
69 produces warmer analyzed SST (0.3 - 0.5 K) over the Atlantic Ocean. Wei et al. (2021a) also reported a warmer analysed
70 lower atmosphere (0.15 K) over Africa and the central Atlantic Ocean in the offline aerosol-aware experiment.

71

72 The experiments conducted in Kim et al. (2018) and Wei et al. (2021a) were based on the application of the CRTM aerosol
73 absorption and scattering routines. While aerosol absorption and scattering options are available from CRTM version 2.2
74 onwards; to our knowledge, the documentation of the CRTM aerosol module (Liu and Lu, 2016) has yet to be updated. Here
75 we presented a joined-up documentation for aerosol absorption and scattering calculations in the CRTM and GSI. In addition,
76 we provide guidance for prospective users of running aerosol-affected GSI analysis. Scientific aspects of aerosol-affected BT
77 in atmospheric data assimilation are also briefly discussed.

78 **2 GSI and CRTM**

79 Below, we provide a brief introduction to the GSI in section 2.1 and a description of the CRTM aerosol option in section 2.2.
80 In section 2.3, a description of running aerosol-aware GSI analysis is given.

81 **2.1 GSI**

82 The multi-partner-developed GSI is an incremental three-dimensional variational (3D-Var) data assimilation system (Wu et
83 al., 2002; Kleist et al. 2009). GSI, alone or combined with an ensemble system, has been used widely by modelling centers
84 and the research community for a range of research and applications. For instance, it is used operationally by the National
85 Oceanic and Atmospheric Administration (NOAA)/National Centers for Environmental Prediction (NCEP) for medium-range
86 weather forecast. It is also used by the National Aeronautics and Space Administration (NASA)/Global Modeling and
87 Assimilation Office (GMAO) for recent production of the Modern-Era Retrospective Analysis for Research and Applications,
88 version 2 (MERRA-2; Gelaro et al., 2017). The community version of the GSI system has been supported and maintained by
89 the Developmental Testbed Center (DTC; <http://www.dtcenter.org>). Note that DTC is scheduled to cease all activities
90 supporting the GSI user community by the end of December 2021. However, community GSI-related assets (website, forum,
91 and repository) built by DTC will remain available to and usable by the community.

92

93 GSI can assimilate a wide range of observations, including conventional observations (such as radiosonde observations), radar
94 data, satellite retrievals (for example global positioning system (GPS) radio occultation sounding data), satellite radiance data,
95 etc. For IR satellite instruments, GSI has the capability to assimilate radiances from Advanced Infrared Sounder (AIRS) on

96 AQUA, Infrared Atmospheric Sounding Interferometer (IASI) on METOP-A and METOP-B, Cross-track Infrared Sounder
97 (CrIS) on S-NPP, High resolution Infrared Radiation Sounder (HIRS) on METOP-A, METOP-B, and NOAA-19, Advanced
98 Very High Resolution Radiometer (AVHRR) on NOAA-18 and METOP-A, Spinning Enhanced Visible and Infrared Imager
99 (SEVIRI) on M08 and M10, and Geostationary Operational Environmental Satellite (GOES) Sounders (sndrD1, sndrD2,
100 sndrD3, and sndrD4) on GOES-15. A comprehensive list of all observations assimilated and monitored by GDAS can be found
101 at the webpage for “Observational Data Processing at NCEP” ([https://www.emc.ncep.noaa.gov/emc/pages/infrastructure/obs-
102 data-processing.php](https://www.emc.ncep.noaa.gov/emc/pages/infrastructure/obs-data-processing.php)).

103

104 Despite the broad applications of GSI, the publicly released version handles only clear-sky radiances for IR sensors. Without
105 correcting for aerosol transmittance effects, systematic biases may be introduced into the meteorological analysis fields when
106 observations affected by aerosols are assimilated. The aerosol-aware option (discussed in section 2.2) reduces such errors by
107 enabling aerosols to influence GSI’s radiance observation operator, CRTM, which calculates the BT and Jacobians (radiance
108 1st derivative). This option, however, may fluctuate the amount of observations assimilated in GSI because the quality control
109 (QC) algorithm screens out observations based on measured BTs and aerosol-free simulated BTs. Thus, an improved QC
110 algorithm is needed to fully exploit radiance measurements under all sky conditions. The technical issues regarding the QC
111 procedure have been discussed in Kim et al. (2018) and Wei et al. (2021a).

112 **2.2 CRTM aerosol module**

113 The CRTM, a one-dimensional radiative transfer model (Liu and Weng, 2006), is developed at the U.S. Joint Center for
114 Satellite Data Assimilation (JCSDA) with algorithm and software input from JCSDA collaborating research institutions. The
115 CRTM is composed of four modules, which include gaseous transmittance, surface emission and reflection, cloud and aerosol
116 absorption and scattering, and a solver for radiative transfer (Han et al., 2006). Given an atmospheric profile of temperature,
117 cloud and surface properties, and gaseous constituents and aerosol concentrations, the CRTM is called within the GSI to
118 calculate BTs for satellite sensors from IR sounders to MW imagers. Here, we describe the aerosol scattering and absorption
119 scheme in CRTM version 2. We refer the readers to Han et al. (2006) for the full details regarding CRTM version 1.

120

121 Absorption by atmospheric trace gases, such as water vapor and carbon dioxide, is parameterized using the Optical Depth in
122 Absorber Space (ODAS) and the Optical Depth in Pressure Space (ODPS) algorithms (Chen et al., 2012), which are based on
123 rigorous line-by-line calculations from the Line-By-Line Radiative Transfer Model (LBLRTM, Clough et al., 1992). ~~For~~
124 ~~enacting aerosol attenuation effects, the CRTM uses Scattering and absorption by aerosols are calculated based on~~ pre-
125 ~~computed lookup tables, containing which calculate~~ aerosol optical properties, ~~specifically the including~~ extinction coefficient,
126 single-scattering albedo, asymmetry factor, and phase function coefficients. ~~Operationally, given aerosol types, radius,~~
127 ~~concentration and ambient relative humidity, CRTM generates aerosol optical profiles that the radiative transfer solver requires~~
128 ~~for multi scattering simulations and radiance calculations.~~ The CRTM version 2.2 and 2.3 contain the optical look-up table

129 ~~that is~~ based on the aerosol types of the mass-based Goddard Chemistry Aerosol Radiation and Transport (GOCART, Chin et
 130 al., 2002; Colarco et al, 2010) module, model for their radiative effects~~the spectrum~~ from the ultraviolet to the infra-red~~IR~~.
 131 Operationally, given aerosol types, radius, concentration and ambient relative humidity, CRTM generates aerosol optical
 132 profiles that the radiative transfer solver requires for multi-scattering simulations and radiance calculations. The effect of
 133 aerosols on MW sensors is not considered yet because the impact of aerosols on MW radiance is usually very small, given
 134 aerosols size is generally much smaller than MW wavelengths (Petty, 2006). There are ongoing and planned CRTM
 135 development efforts to incorporate more aerosol optical tables (such as the Community Multiscale Air Quality model, CMAQ).
 136 With the expansion of the aerosol schemes, a new releasing and versioning system for optical tables is essential and currently
 137 under discussion. This article, however, discusses mainly the GOCART model, which is the default aerosol scheme in the
 138 CRTM version 2.

139
 140 The GOCART model (Chin et al., 2002; 2014), a bulk aerosol scheme, simulates major tropospheric aerosol components,
 141 including dust, sea salt, black carbon (BC), organic carbon (OC) and sulfate. It is one of the most widely used aerosol modules
 142 in the Weather Research and Forecasting model coupled with Chemistry (WRF-Chem; see Ukhov et al. (2021) and references
 143 therein). It is used in the GEOS framework at GMAO for near-real-time aerosol forecasts (Colarco et al., 2010) as well as in
 144 MERRA reanalysis (Bucharad et al., 2015) and MERRA-2 reanalysis (Randles et al., 2017). It is also implemented in the Global
 145 Forecast System (GFS) framework at NCEP (Lu et al., 2016; Wang et al., 2018; Zhang et al., 2021) for near-real-time global
 146 aerosol forecasts.

147
 148 When GOCART was selected as the aerosol module within WRF-Chem, it was configured with fourteen GOCART aerosol
 149 species (Liu et al., 2011): sulfate; hydrophobic and hydrophilic OC and BC; sea salt in four particle size bins (with radii of
 150 0.1-0.5, 0.5-1.5, 1.5-5, and 5-10 μm) and dust particles in five particle size bins (with radii of 0.1-1.0, 1.0-1.8, 1.8-3, 3-6, and
 151 6-10 μm). A default CRTM lookup-table has been used for pre-calculated aerosol optical property parameters for the fourteen
 152 GOCART aerosol species (Liu et al., 2007; Liu and Lu, 2016). We assume that the particles are spherical and externally mixed.
 153 We also assume lognormal size distributions for sulfate and carbonaceous aerosols as well as for each sea salt and dust bin.
 154 The lognormal size distribution for N particles can be expressed as follows (d’Almeida et al., 1991),

$$155 \quad n(\ln r) = \frac{N}{\sqrt{2\pi} \ln(\sigma_g)} \exp\left[-\frac{1}{2} \left(\frac{\ln r - \ln r_g}{\ln(\sigma_g)}\right)^2\right], \quad (1)$$

156 where r is a radius, r_g the geometric median radius, and σ_g the geometric mean standard deviation. The k^{th} moment of the
 157 distribution can be expressed as follows (Binkowski and Roselle, 2003),

$$158 \quad M_k = \int_{-\infty}^{\infty} r^k n(\ln r) d\ln(r) = r_g^k \exp\left[\frac{k^2}{2} \ln^2(\sigma_g)\right]. \quad (2)$$

159 where M_0 is the number N of aerosol particles, and M_2 and M_3 are proportional to the total particulate surface area and volume,
 160 respectively. Thus, the effective radius (r_{eff}) can be defined as

$$r_{eff} = \frac{M_3}{M_2} = r_g \exp\left[\frac{5}{2} \ln^2(\sigma_g)\right] \quad (3)$$

161
 162
 163 Table 1 lists the GOCART size parameters (particle density, effective radius, and geometric standard deviation) and refractive
 164 indices at 550 nm used in CRTM version 2. The optical properties of each aerosol species are computed based on Mie scattering
 165 theory. Hydrophilic aerosol particle size increases as relative humidity (RH) of the ambient atmosphere increases. Therefore,
 166 the water content in aerosol needs to be considered when calculating the refractive index. The effective radius growth factor
 167 for hygroscopic aerosols may be theoretically calculated or obtained from a pre-calculated look-up table (d’Almeida et al.,
 168 1991). In this study, the hygroscopic growth factor used for the GOCART model (Chin et al., 2002) is adopted and given in
 169 Table 2. Once the growth factor a_g is evaluated, the refractive index n_r for the hygroscopic aerosol can be calculated using a
 170 volume mixing method as:

$$n_r = n_w + (n_o - n_w) \times a_g^3 \quad (4)$$

171
 172 where n_o and n_w are the refractive indices for dry aerosols and water, respectively. We adopt the refractive index n_o from the
 173 Optical Properties of Aerosols and Clouds (OPAC) dataset (Hess et al. 1998), while the water refractive index is given by
 174 (Hale and Querry, 1973).

175
 176 **Table 1.** Goddard Chemistry Aerosol Radiation and Transport (GOCART) size distribution parameters and refractive indices
 177 at 550 nm for dry aerosols.

Aerosol type	Density [g cm ⁻³]	Effective radius r_{eff} [μm]	Standard deviation σ [μm]	Refractive index real part $n(\lambda)$	Refractive index imaginary part $k(\lambda)$
Sulfate	1.7	0.242	2.03	1.43	1.00×10^{-8}
OC1 (hydrophobic)	1.8	0.087	2.20	1.53	6.00×10^{-3}
OC2 (hydrophilic)	1.8	0.087	2.20	1.53	6.00×10^{-3}
BC1 (hydrophobic)	1.0	0.036	2.0	1.75	4.40×10^{-1}
BC2 (hydrophilic)	1.0	0.036	2.0	1.75	4.40×10^{-1}
SeaSalt1 (size range)	2.2	0.3	2.03	1.50	1.00×10^{-8}
SeaSalt2	2.2	1.0	2.03	1.50	1.00×10^{-8}
SeaSalt3	2.2	3.25	2.03	1.50	1.00×10^{-8}
SeaSalt4	2.2	7.5	2.03	1.50	1.00×10^{-8}
Dust1 (size range)	2.6	0.65	2.0	1.53	5.50×10^{-3}
Dust2	2.6	1.4	2.0	1.53	5.50×10^{-3}
Dust3	2.6	2.4	2.0	1.53	5.50×10^{-3}

Dust4	2.6	4.5	2.0	1.53	5.50×10^{-3}
Dust5	2.6	8.0	2.0	1.53	5.50×10^{-3}

178

179

Table 2. Hygroscopic aerosol growth factor ag as a function of the ambient relative humidity (RH).

RH(%)	0	50	70	80	90	95	99
Sulfate	1.0	1.4	1.5	1.6	1.8	1.9	2.2
Organic Carbon	1.0	1.2	1.4	1.5	1.6	1.8	2.2
Black Carbon	1.0	1.0	1.0	1.2	1.4	1.5	1.9
Sea Salt	1.0	1.6	1.8	2.0	2.4	2.9	4.8

180

181

182

183

184

185

186

187

188

189

The GOCART model used by GMAO and NCEP for aerosol forecast and reanalysis has evolved to use 5 sea salt size bins (with radii of 0.03-0.1, 0.1-0.5, 0.5-1.5, 1.5-5, and 5-10 μm). The first sub-micron sea salt bin was added to facilitate optical properties and aerosol-cloud interaction studies (Colarco et al., 2010), but was excluded from the previous GOCART versions as well as the WRF-Chem GOCART model. While GMAO's GEOS and NCEP's GFS contain fifteen GOCART aerosol species, the CRTM aerosol module has also not yet been modified to include the new added sub-micron sea salt bin (see Table 1). To overcome this discrepancy, the latest GSI/CRTM release (i.e., GSI 3.7 and CRTM 2.3) combines the mixing ratios from the two sub-micron sea salt bins in order to use the aerosol optical property parameters from the original GOCART model. This limitation is acknowledged in this article and will be addressed in a future CRTM release (see section 4).

190

191

192

193

194

While the CRTM is primarily designed for computing satellite radiances, an additional module was added to CRTM by Liu and Lu (2016) to compute aerosol optical depth (AOD). This CRTM-AOD module enables the GSI system to assimilate AOD observations (Liu et al., 2011; Schwartz et al., 2012; Pagowski et al., 2014). This article, however, is focused on the observation operator for radiance, and we refer the reader to Pagowski et al. (2014) for the description of the AOD observation operator and GSI AOD data assimilation.

195

2.3 Running aerosol-aware GSI analysis

196

197

198

199

200

201

The operational version of GSI maintained by NOAA/NCEP Environmental Modeling Center (EMC) is utilized in the present study. Its source code and associated static files are distributed through the GitHub repository (<https://github.com/NOAA-EMC/GSI>). An open-access archive of source code and data is described in Code and Data Availability. To run the GSI analysis, the reader can refer to the user guide for GSI v3.7 (the latest released version as of April 2021), which is available at https://dtcenter.ucar.edu/com-GSI/users/docs/users_guide/html_v3.7/index.html. In addition, an online tutorial is available at https://dtcenter.ucar.edu/com-GSI/users/tutorial/online_tutorial/index_v3.7.php. For CRTM, the user guide and tutorials can

202 be found at <https://www.jcsda.org/jcsda-project-community-radiative-transfer-model>. Thus, only a brief description of
203 aerosol-affected BT calculations is given.

204

205 A regression test “global_C96_fv3aerorad” has been introduced into NOAA/EMC GSI code repository (pull request #32) to
206 assure the functionality of aerosol-aware BT derivations in GSI/CRTM works as expected. This regression test uses a sample
207 background file taken from the aerosol member of the Global Ensemble Forecast System (GEFS-Aerosol; Zhang et al., 2021).
208 All fifteen GOCART aerosol species are passed along to the CRTM. In addition to the background file, a user needs to modify
209 the configuration files, anavinfo and satinfo, in the “fix” directory. The anavinfo file is the information file to set control and
210 analysis variables. The satinfo file is the information file to specify satellite channels to be assimilated and associated
211 parameters. For an aerosol-aware experiment where aerosol absorption and scattering are included in BT calculations, aerosol
212 species are specified in the “chem_guess” section of anavinfo and sensors and channels are set to 1 in the “iaerosol” column
213 of satinfo. The reader can refer to the fv3aerorad_satinfo.txt and anavinfo_fv3aerorad for the aerosol-aware configuration. The
214 corresponding namelist (gsiparm.anl) can be found at the “global_C96_fv3aerorad” section (line 2931–3046) in
215 regression_namelists.sh under the “regression” directory. It should be noted that the namelist variable, “lread_ext_aerosol”,
216 determines how GSI ingests the aerosol information from background files or external files.

217 **3. Numerical Results**

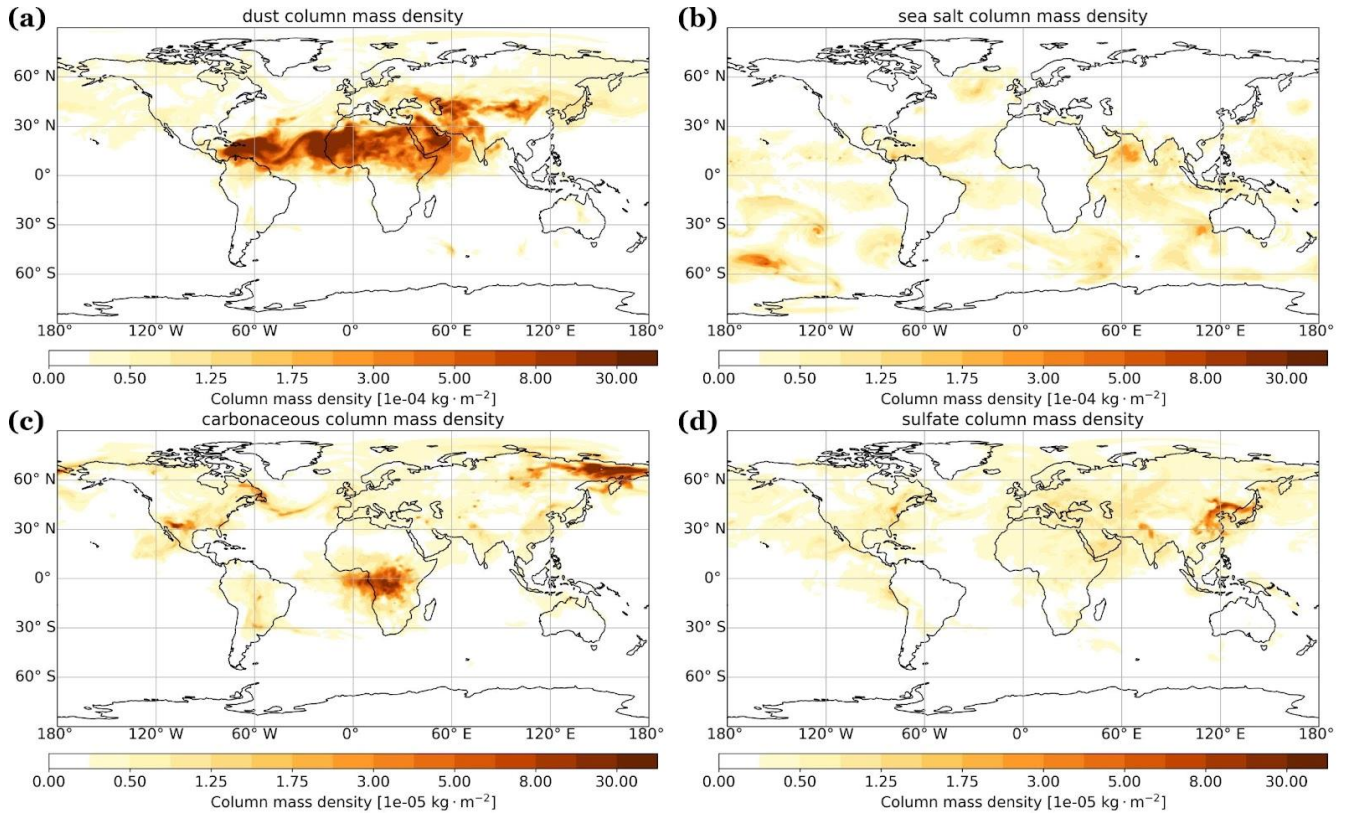
218 **3.1 Aerosol impacts on BT calculations**

219 To illustrate how an aerosol transmittance correction is required within satellite radiances assimilated into meteorological data
220 assimilation systems, we present a detailed analysis of a single-cycle GSI experiment (the AER experiment) using GOCART
221 fields from MERRA-2 on 12Z June 22, 2020. This time is chosen because it captures a strong Saharan dust event that covers
222 the trans-Atlantic region. A baseline GSI experiment (the CTL experiment) with the anavinfo and satinfo resource files reverted
223 back to the default aerosol-blind configuration was also conducted. Both experiments used the same first-guess fields and
224 assimilated identical conventional and satellite observations within a ± 3 -hour assimilation window. In AER, the aerosol
225 transmittance effects were only considered in the CRTM simulation for IR sensors.

226

227 Figure 1 shows the global aerosol column mass density distribution from MERRA-2 during 12Z June 22, 2020. The panels a,
228 b, c, and d depict dust, sea salt, carbonaceous and sulfate, respectively. Dust plumes spread over northern Africa, the tropical
229 Atlantic Ocean, the Middle East, and northwestern China. Wind-driven sea salt aerosols are seen over tropical and southern
230 hemisphere oceans. Carbonaceous and sulfate aerosols mainly appear in areas with extensive biomass burning and fuel
231 combustion activities (note one order smaller than dust and sea salt). The overall aerosol loading is dominated by mineral dust.
232 Wu et al. (2020) evaluated the dust spatiotemporal variations of MERRA-2 against satellite observations and global model
233 simulations. They found that MERRA-2 agrees well with satellite observations due to the assimilation of satellite AOD. But

234 in North America and the Arctic, the dust burden in MERRA-2 is much larger than those in other models despite having similar
 235 dust emissions fluxes. The high dust burden over these regions is due to higher mass fraction of fine dust and enhanced dust
 236 transport. Furthermore, Bullard et al. (2016) reported that large gaps exist in our understanding of basic characteristics of high-
 237 latitude dust sources. This highlights the importance of representing aerosol emissions, transport, removal, and size distribution
 238 in global models in correctly simulating aerosol spatiotemporal distributions.
 239

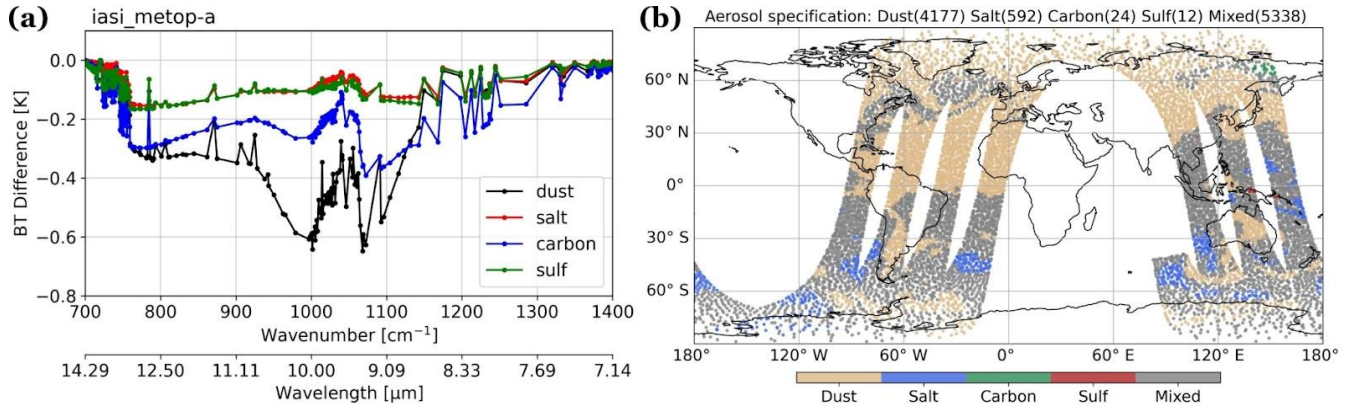


240
 241 **Figure 1.** Aerosol column mass density (kg m^{-2}) from MERRA-2 on 12Z June 22, 2020: (a) dust, (b) sea salt, (c) carbonaceous,
 242 and (d) sulfate.

243
 244 Figure 2a shows the first-guess BT differences of IASI onboard METOP-A between the two experiments (AER – CTL) in the
 245 IR atmospheric window channels over dust, sea salt, carbonaceous and sulfate dominant regions. The stratification criterion
 246 for each type is where the fraction of column mass density of dominant species, from MERRA-2, is larger than 0.65 (shown
 247 in Fig. 2b). Figure 2a shows that dust aerosols generate the stronger cooling effects, about 0.7 K at the thermal IR window
 248 region ($\sim 10 \mu\text{m}$), than other species. The importance of correcting for aerosol transmittance effects within BT algorithms has
 249 been reported in previous studies (Sokolik, 2002; Weaver et al., 2003; Pierangelo et al., 2004; Matricardi, 2005; Merchant et
 250 al., 2006; Kim et al., 2018; Wei et al., 2021a). Table 3 describes the range and the average of total aerosol column mass density

251 over the regions with different dominant aerosol species. It shows that the total loading of aerosols is similar over the dust and
 252 carbonaceous aerosols dominated regions. This indicates that the stronger cooling effects by dust aerosol on BT in the IR
 253 window region is not due to stronger loading. Note that in the northern hemisphere, the high-latitude region is characterized
 254 as dust-dominant except for the Russian Far East in MERRA-2 (Figure 2b). While anomalous or erroneous modeled aerosol
 255 loading may bias the results, the finding that dust has the largest impact on the BTs simulations, reported in this study and
 256 previous studies, remains unchanged. Therefore, we focus our remaining analysis on dust over Tropical Africa and the Mid-
 257 Atlantic.

258
 259



260
 261
 262
 263
 264

Figure 2. (a) The differences (AER-CTL) of first-guess brightness temperatures in the IR window region of IASI onboard METOP-A. (b) The corresponding regions dominated by different aerosol species from the 12Z June 22, 2020. The data counts for each species are labelled in panel (b).

265
 266

Table 3. The range of aerosol column mass density (kg/m^2) from MERRA-2 at the regions dominated by different aerosol species (fraction over 0.65) of IASI onboard METOP-A at the cycle of 12Z June 22, 2020.

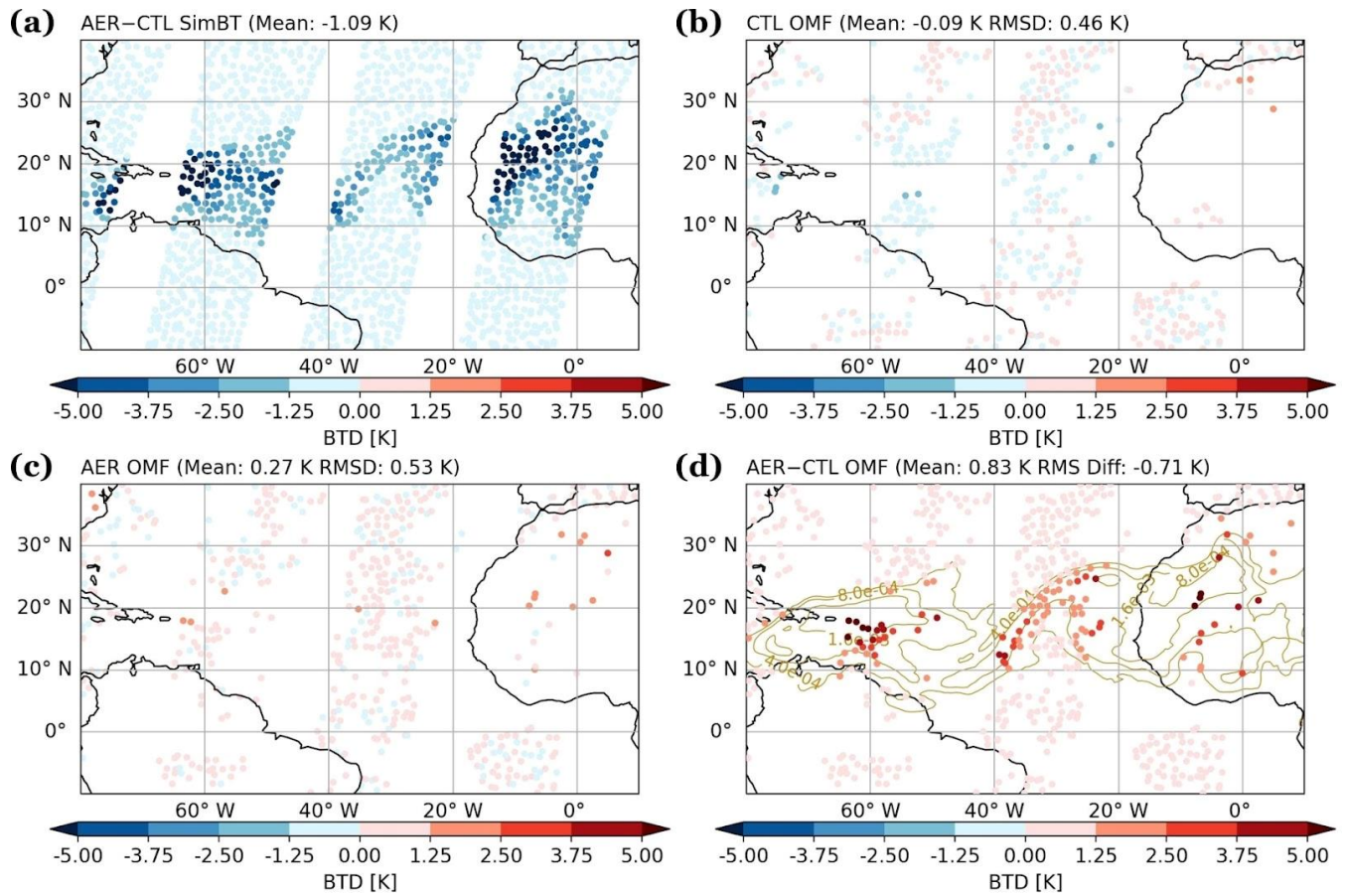
Dominant aerosol species	Column mass density (kg/m^2)				
	Minimum	Maximum	Mean	Median	SD
Dust	2.69e-06	2.88e-03	1.76e-04	4.20e-05	3.59e-04
Sea salt	4.91e-06	4.01e-05	1.68e-05	1.59e-05	6.15e-06
BC+OC	1.04e-05	6.07e-04	1.76e-04	1.52e-04	1.20e-04
Sulfate	6.45e-06	9.53e-05	2.15e-05	1.28e-05	2.46e-05

267

268 Figure 3 displays the AER - CTL difference in the simulated BTs and their respective first-guess departures (observed minus
269 first guess, OMF) calculated at the 10.39 μm channel from IASI onboard METOP-A. The Figure focuses on North Africa and
270 the trans-Atlantic region, where a large dust plume spans the region. Significant aerosol cooling (~ 4 K) in BT was found in
271 the aerosol-aware experiment (Fig. 3a) due to the large plume. Comparing the first guess departures from CTL and AER
272 experiments (Fig. 3b and 3c) shows that OMFs for AER are warmer than CTL (cf. 0.27 K vs. -0.09 K). Note that some
273 observations assimilated in CTL were rejected in AER (near 55° W and 15° N) and vice versa (near 65° W and 15° N, and
274 over Africa). This feature suggests that the quality control has been influenced by including aerosol transmittance effects in
275 CRTM. Over the trans-Atlantic region, the aerosol-aware experiment assimilated several observations with larger first-guess
276 departures located in the strong dust plume (Fig. 3d). Figure 4 presents the scatter plot of dust column mass density versus
277 OMF differences (AER - CTL) for these data points assimilated in AER on 12Z June 22, 2020. The data points with large
278 OMF differences are corresponding to the areas with higher dust loading. Nevertheless, when considering aerosol information,
279 the root-mean-square first-guess departures decreased 0.08 K globally and 0.42 K over the trans-Atlantic region at this channel
280 (not shown here). This implies that simulated BTs in the aerosol aware run are in better agreement with the observations.

281

282



283

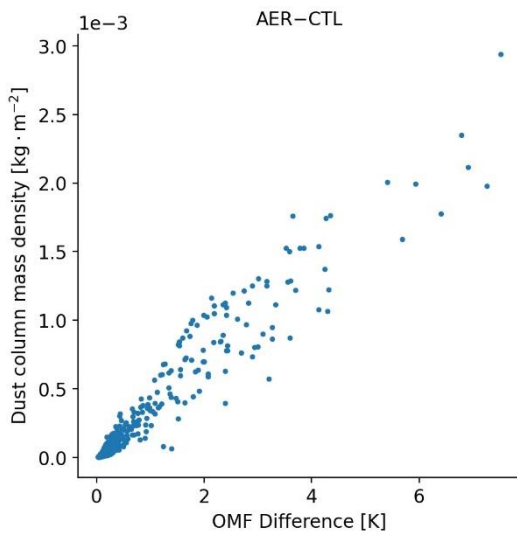
284

285

286

287

Figure 3. (a) Simulated BT differences (AER – CTL), (b) bias-corrected OMF from the CTL experiment, (c) bias-corrected OMF from the AER experiment, and (d) OMF differences (AER – CTL) for 10.39 μm channel of IASI onboard METOP-A. All the data are from the analysis cycle on 12Z June 22, 2020. Contours of total column mass density from MERRA-2 are plotted in panel (d).



288

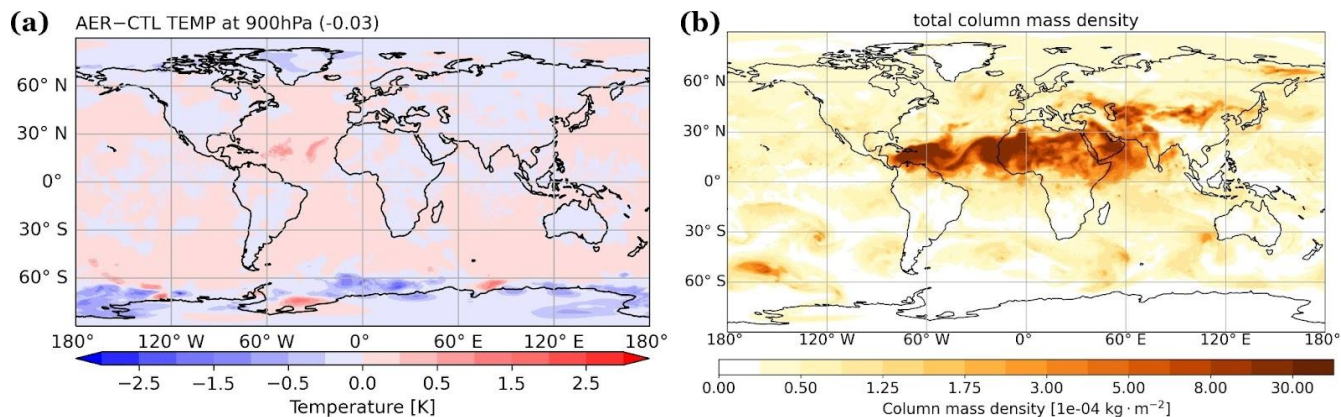
289 **Figure 4.** The scatter plot of dust column mass density from MERRA-2 against the first-guess departure differences (AER –
 290 CTL) assimilated in AER experiment (without bias correction) on 12Z June 22, 2020.

291

292 Figure 5 shows (a) the global differences in analyzed temperature at 900 hPa between the two experiments and (b) the total
 293 aerosol column mass density incorporated in the GSI/CRTM system. When aerosol transmittance effects are considered in the
 294 BT calculations, the air temperatures are not only adjusted over aerosol-laden regions but also across the globe. The impact is
 295 shown outside aerosol-active regions, which could be attributed to the change from the spatial correlation in the GSI
 296 background error covariance. Over the trans-Atlantic region where the dust loading is high (shown in Figure 1a), the AER
 297 experiment produces 0.5 K to 1 K of warming relative to CTL. As dust travels off the west coast of Africa into the Atlantic,
 298 the particles are lifted and carried by the Saharan Air Layer (SAL), around 800 – 600 hPa (Diaz et al., 1976; Karyampudi et
 299 al., 1999). In the case of 12Z June 22, 2020, MERRA-2 captured the dust transport within SAL, and air mass is increasingly
 300 composed of fine dust particles due to the gravitational settling of coarser particles (not shown here). Wei et al. (2021b)
 301 conducted a series of CRTM v2.3 experiments using idealized dust profiles and reported that mass loading and the altitude of
 302 the dust layer are the primary and secondary factors affecting the BT simulations, respectively; changes in the fine versus
 303 coarse particle partition show little influence on the BT simulations. Based on these results we speculate that elevated dust
 304 plume retains unneglected influences on BT calculations (Figure 3a). Experiments with robust estimated aerosol distributions
 305 over extended time period are needed to quantify the sensitivity of GSI analysis to aerosol-aware CRTM calculations. This
 306 manuscript, however, is intended to provide a joined-up documentation for the CRTM aerosol option and thus unravelling
 307 these questions is beyond the scope of this study.

308

309

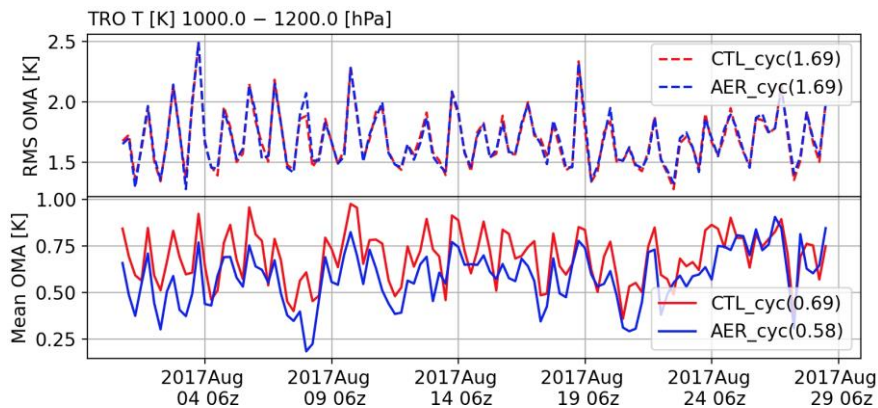


310
 311 **Figure 5.** (a) The differences (AER - CTL) of analyzed temperature (K) at 900 hPa and (b) the corresponding aerosol column
 312 mass density (kg m^{-2}) from MERRA-2 on 12Z June 22, 2020.

313 3.2 Aerosol impacts on the analysis

314 The experiments reported in this section were produced with the NCEP GFS version 14 and the corresponding GDAS. Our
 315 experiments used a coarser resolution, T670 (~ 30 km) for the model and T254 (~ 80 km) for the analysis, different from the
 316 NCEP operational GFSv14 configuration at T1534 (~ 13 km) and T574 (~ 27 km). The experiments covered the August 2017
 317 period, initialized from NCEP's archived GDAS analysis on July 25 00Z. The analysis cycles every 6 hours (at 00z, 06z, 12z,
 318 and 18z), with a ± 3 -hour assimilation window and continuous data utilization. The control experiment (CTL_cyc) was an
 319 aerosol-blind fully cycled experiment where aerosol effects on radiances are not considered (as is by default). The aerosol
 320 experiment (AER_cyc) was an aerosol-aware fully cycled experiment where aerosol-affected satellite radiances are taken into
 321 account. Here, we used CRTM version 2.2.4. Time-varying 3-dimensional GOCART aerosols were taken from NCEP's
 322 archived NEMS GFS Aerosol Component (NGAC) v2 (Wang et al., 2018).

323
 324 Figure 6 displays the statistics of analysis departures (observation minus analysis, OMA) from CTL_cyc and AER_cyc to
 325 evaluate the performance of temperature analysis at the lower atmosphere over the tropical region ($20^\circ \text{S} - 20^\circ \text{N}$). The positive
 326 value of mean OMAs indicates that both experiments have cold biases in the tropical region. It shows neutral impact on root-
 327 mean-square (RMS) and slightly positive impact on the cold biases. The latter implies that the departure of temperature analysis
 328 becomes larger when considering aerosol transmittance effects during the data assimilation (i.e., AER_cyc).



330

331 **Figure 6.** The comparison of the RMS and mean analysis departures (observation minus analysis, OMA) against in-situ
 332 measurements (e.g., radiosonde) of temperature with pressure over 1,000 hPa at the tropical region (20° S – 20° N) during 00Z
 333 August 1 – 18Z August 28, 2017.

334

335 Medium-range forecasts of AER_cyc are examined against CTL_cyc using the verification package from NOAA/NCEP EMC
 336 (https://www.emc.ncep.noaa.gov/gmb/STATS_vsdb). Figure 7 displays the scorecard of anomaly correlation and root-mean-
 337 square error (RMSE) for the day-1, -3, and -5 forecasts over August 1 – 28, 2017. Anomaly correlation coefficients show
 338 neutral to positive impact on day-1 forecasts of wind and temperature fields when aerosol cooling effects in BTs are considered.
 339 The RMSE scorecards show the forecast improvements in the wind, temperature and height fields throughout the troposphere
 340 over the Tropics (20° S – 20° N) and at upper level over the Northern Hemisphere (20° N – 80° N). For the Southern hemisphere
 341 (20° S – 80° S), however, there is neutral impact or degradation in the forecasts, which is likely due to cloud contamination
 342 and mixture of sea salt and aged smoke/sulfate aerosols. Compared to both hemispheres, the tropical forecasts show the most
 343 improved statistics in the aerosol-aware analysis, which may be attributed to larger aerosol loading in this region. While the
 344 RMSE scorecard focuses on background (i.e., time-averaged) fields, it should be noted that evaluation of the aerosol impacts
 345 on the analysis and forecasts of African easterly wave that developed Hurricane Harvey and Gert in 2017 is presented in
 346 Grogan et al. (2021).

347

		Globe			N. Hemisphere			S. Hemisphere			Tropics					
		Day 1	Day 3	Day 5	Day 1	Day 3	Day 5	Day 1	Day 3	Day 5	Day 1	Day 3	Day 5			
Anomaly Correlation	Heights	250hPa														
		500hPa														
		700hPa														
		1000hPa														
	Vector Wind	250hPa	▲													
		500hPa	▲													
		850hPa	▲													
	Temp	250hPa	▲													
		500hPa		▼							▼					
		850hPa	▲													
RMSE	Heights	10hPa	▲	▲	▲		▲	▲	▲				▲	▲	▲	
		20hPa	▲	▲	▲	▲	▲	▲					▲	▲	▲	
		50hPa	▲	▲	▲	▲	▲	▲	▲	▲				▲	▲	▲
		100hPa	▲	▲	▲	▲	▲	▲	▲	▲				▲	▲	▲
		200hPa	▲											▲	▲	▲
		500hPa												▲	▲	▲
		700hPa														
		850hPa														
		1000hPa														
		Vector Wind	10hPa	▲	▲		▲	▲	▲						▲	▲
	20hPa		▲	▲		▲	▲	▲	▲	▲	▲	▲		▲	▲	▲
	50hPa		▲	▲	▲	▲	▲	▲	▲	▲	▲			▲	▲	▲
	100hPa		▲	▲	▲	▲	▲	▲	▲	▲	▲	▲		▲	▲	▲
	200hPa		▲			▲								▲	▲	
	500hPa		▲											▲	▲	
	700hPa		▲											▲	▲	
	850hPa		▲											▲	▲	
	1000hPa		▲											▲	▲	
	Temp		10hPa	▲	▲		▲	▲	▲						▲	▲
		20hPa	▲	▲		▲	▲	▲	▲	▲	▲			▲	▲	▲
		50hPa	▲	▲		▲	▲	▲	▲	▲	▲	▲		▲	▲	▲
		100hPa	▲	▲	▲	▲	▲	▲	▲	▲	▲			▲	▲	▲
		200hPa	▲			▲								▲	▲	▲
		500hPa														
		700hPa														
		850hPa	▲			▲								▲	▲	
		1000hPa	▲			▲								▲	▲	

348

349

350

351

352

353

Figure 7. Scorecard of anomaly correlation and RMSE of comparison between AER_cyc and CTL_cyc. Green colors mean AER_cyc is better than CTL_cyc at 95% (filled box), 99% (▲), and 99.9% (▲) significance level. Red colors mean AER_cyc is worse than CTL_cyc at 95% (filled box), 99% (▼), and 99.9% (▼) significance level. Grey boxes mean no statistically significant difference between AER_cyc and CTL_cyc. Blue boxes are not statistically relevant. The statistics are calculated between 20 to 80 degrees of latitude for both hemispheres. The data between 20°S and 20°N is used for the tropical region.

354

4. Conclusions and Future Outlook

355

356

357

This article described aerosol absorption and scattering calculations of the CRTM version 2 in the GSI analysis. We also conducted sensitivity experiments to investigate the aerosol-affected GSI analysis in both single-cycle and fully-cycled runs. Both GSI and CRTM are well documented with user guides, tutorials and code repositories available online. This article is

358 primarily a joined-up documentation for aerosol absorption and scattering calculations in the CRTM version 2 and GSI. It also
359 provides guidance for prospective users of the CRTM aerosol option. Scientific aspects of aerosol-affected BT in atmospheric
360 data assimilation are briefly discussed. Specifically, numerical experiments were conducted to illustrate how including aerosol
361 radiative effects in CRTM changes the GSI analysis. We found that taking the aerosols into account reduces simulated BT in
362 thermal window channels over dust-dominant regions. Assimilating aerosol-affected BTs produces a warmer analyzed lower
363 atmosphere. From the verification scorecard, neutral to positive results are found in the fully-cycled, aerosol aware experiment.
364

365 The CRTM team, in coordination with its partners and collaborators, is building a robust capability to accurately and
366 consistently simulate the emission, absorption, and scattering properties of all (radiatively important) atmospheric constituents.
367 There are several ongoing and planned efforts to enhance the CRTM aerosol module. For example, more aerosol optical look-
368 up tables have been added and the calculations of aerosol optical properties are being evaluated. In addition, the CRTM is
369 being refactored toward a more flexible aerosol interface to handle aerosol optical look-up-tables as well as to support aerosol
370 specifications from other operational aerosol models, such as Community Multiscale Air Quality (CMAQ). Other aerosol-
371 related efforts include, but are not limited to, improving the physical representation of aerosols and including active sensors
372 such as aerosol lidar. These developments, once implemented and tested, will be reported in future manuscripts.

373 **Code and Data Availability.**

374 Various software packages are referred to throughout the paper. The following list contain links to the main software
375 documentations or repositories discussed:

376 The GSI webpage: <https://dtcenter.ucar.edu/com-GSI/users/index.php>

377 The GSI v3.7 user guide: https://dtcenter.ucar.edu/com-GSI/users/docs/users_guide/html_v3.7/index.html

378 The GSI v3.7 online tutorial: https://dtcenter.ucar.edu/com-GSI/users/tutorial/online_tutorial/index_v3.7.php

379 The DTC community GSI (as of Nov. 29, 2021, via Zenodo): <https://doi.org/10.5281/zenodo.5735601>

380 The CRTM v2.3.0 public repository (via Zenodo): <https://doi.org/10.5281/zenodo.5695707>

381 The aerosol related Fortran code in GSI:

382 Aerosol files check (when lread_ext_aerosol is true): `./src/gsi/read_files.f90`

383 Aerosol data ingestion: `./src/gsi/ncepnmemo_io.f90`, `./src/gsi/general_read_nemsaero.f90`

384 CRTM simulation: `./src/gsi/crtm_interface.f90`

385 Effective radius setup: `./src/gsi/set_crtm_aerosolmod.f90`

386 **Author Contributions.**

387 QL implemented the aerosol module, CL designed the experiments, and SW performed the experiments. CL prepared the
388 manuscript with contributions from all co-authors.

389 **Acknowledgements.**

390 The study of CTL and AER cycled experiments are supported by the Next Generation Global Prediction System (NGGPS)
391 program within NOAA/NWS (award number 352 NA15NWS4680008). The testing and refinement of GSI/CRTM regression
392 test is supported by the DTC Visitor Program. All experiments were conducted at NOAA/NESDIS-funded Supercomputer for
393 Satellite Simulations and Data Assimilation Studies (S4) cluster maintained by Space Science and Engineering Center (SSEC)
394 at University of Wisconsin-Madison. We thank GMAO collaborators, Arlindo da Silva, Mian Chin, and Peter Colarco, for
395 providing valuable input on the calculations of aerosol optical properties for GOCART aerosols.

396 **References**

- 397 d'Almeida, G. A., Koepke, P., and Shettle, E.P.: Atmospheric Aerosols: global climatology and radiative characteristics, A.
398 Deepak Publishing, Hampton, VA., 1991.
- 399 American Meteorological Society: Brightness Temperature. Glossary of Meteorology,
400 https://glossary.ametsoc.org/wiki/Brightness_temperature, 2012.
- 401 Binkowski, F. S., Roselle, S. J.: Models-3 Community multiscale air quality (CMAQ) model aerosol component, 1 Model
402 description. *J. Geophys. Res.*, 108, 4183, doi:10.1029/2001JD001409, 2003.
- 403 Buchard, V., da Silva, A. M., Colarco, P. R., Darmonov, A., Randles, C. A., Govindaraju, R., Torres, O., Campbell, J., and
404 Spurr, R.: Using the OMI aerosol index and absorption aerosol optical depth to evaluate the NASA MERRA Aerosol
405 Reanalysis. *Atmos. Chem. Phys.*, 15, 5743–5760, doi:10.5194/acp-15-5743-2015, 2015.
- 406 Bullard, J. E. and Coauthors: High-latitude dust in the Earth system, *Rev. Geophys.*, 54, 447–485, doi:10.1002/
407 2016RG000518, 2016.
- 408 Chen, Y., Weng, F., Han, Y., and Liu, Q.: Planck-Weighted Transmittance and Correction of Solar Reflection for Broadband
409 Infrared Satellite Channels. *J. Atmos. Sci.* 29, 382-396, 2012.
- 410 Chin, M., Ginoux, P., Kinne, S., Torres, O., Holben, B. N., Duncan, B. N., Martin, R. V., Logan, J. A., and Higurashi, A.:
411 Tropospheric aerosol optical thickness from the GOCART model and comparisons with satellite and Sun photometer
412 measurements, *J. Atmos. Sci.*, 59, 461–483, doi:10.1175/1520-0469(2002)059<0461:TAOTFT>2.0.CO;2, 2002.
- 413 Chin, M., Diehl, T., Tan, Q., Prospero, J. M., Kahn, R. A., Remer, L. A., Yu, H., Sayer, A. M., Bian, H., Geogdzhayev, I. V.,
414 Holben, B. N., Howell, S. G., Huebert, B. J., Hsu, N. C., Kim, D., Kucsera, T. L., Levy, R. C., Mishchenko, M. I., Pan, X.,
415 Quinn, P. K., Schuster, G. L., Streets, D. G., Strode, S. A., Torres, O., and Zhao, X.-P.: Multi-decadal aerosol variations

416 from 1980 to 2009: a perspective from observations and a global model, *Atmos. Chem. Phys.*, 14, 3657–3690,
417 doi.org:10.5194/acp14-3657-2014, 2014.

418 Clough, S., Iacano, M. J. and Moncet, J.-L.: Line-by-line Calculations of Atmospheric Fluxes and Cooling Rates: Application
419 to Water Vapor. *J. Geophys. Res.* 97, 15761-15785, 1992.

420 Colarco, P., da Silva, A., Chin, M., and Diehl, T.: Online simulations of global aerosol distributions in the NASA GEOS-4
421 model and comparisons to satellite and ground-based aerosol optical depth, *J. Geophys. Res.*, 115, D14207,
422 doi:10.1029/2009JD012820, 2010.

423 Diaz, H. F., Carlson, T. N., and Prospero, J. M.: A study of the structure and dynamics of the Saharan air layer over the northern
424 equatorial Atlantic during BOMEX. National Hurricane and Experimental Meteorology Laboratory NOAA Tech. Memo.
425 ERL WMPO-32, 61 pp, 1976.

426 Diaz, J. P., Arbelo, M., Expósito, F.J., Podesta', G., Prospero, J.M., and Evans, R.: Relationship between errors in AVHRR-
427 derived sea surface temperature and the TOMS Aerosol Index, *Geophys. Res. Lett.*, 28, 1989 – 1992, 2001.

428 Divakarla, M., and Coauthors: Evaluation of CrIMSS operational products using in-situ measurements, model analysis fields,
429 and retrieval products from heritage algorithms, IEEE International Geoscience and Remote Sensing Symposium, Munich,
430 Germany, 2012, pp. 1046-1049, doi: 10.1109/IGARSS.2012.6350818, 2012.

431 Gelaro, R., McCarty, W., Suarez, M. J., Todling, R., and coauthors, 2017: The Modern-Era Retrospective Analysis for
432 Research and Applications, Version 2 (MERRA-2). *J. Climate*, 30, 5419–5454, doi.org: 10.1175/JCLI-D-16-0758.1, 2017.

433 Grogan, D., Lu, C.-H., Wei, S.-W., and Chen, S.-P.: Effects of Saharan dust on African easterly waves: The impact of aerosol-
434 affected satellite radiances on data assimilation, *Atmos. Chem. Phys. Disc.*, doi:10.5194/acp-2021-129, 2021.

435 Hale, G. M. and Querry, M. R.: Optical constants of water in the 200-nm to 200-mm wavelength region. *Appl. Opt.*, 12, 555–
436 563, 1973.

437 Han, Y., van Delst, P., Liu, Q., Weng, F., Yan, B., Treadon, R., and Derber, J.: JCSDA Community Radiative Transfer Model
438 (CRTM) – Version 1, NOAA NESDIS Tech. Rep. 122, 33 pp., NOAA, Silver Spring, Md, 2006.

439 Han, Y., Weng, F., Liu, Q., and van Delst, P.: A fast radiative transfer model for SSMIS upper atmosphere sounding channels.
440 *J. Geophys. Res.*, 112, D11121, doi:10.1029/2006JD008208, 2007.

441 Hess, M., Koepke, P., Schult I: Optical properties of aerosols and clouds: the software package 1528 OPAC. *Bull Am Met Soc*
442 79:831–844, 1998.

443 Highwood, E. J., Haywood, J. M., Silverstone, M. D., Newman, S. M., and Taylor, J. P.: Radiative properties and direct effect
444 of Saharan dust measured by the C-130 aircraft during Saharan Dust Experiment (SHADE): 2. Terrestrial spectrum, *J.*
445 *Geophys. Res.*, 108(D18), 8578, doi:10.1029/2002JD002552, 2003.

446 Karyampudi, V. M., Palm, S. P., Reagen, J. A., Fang, H., Grant, W. B., Hoff, R. M., Moulin, C., Pierce, H.
447 F., Torres, O., Browell, E. V., and Melfi, S. H.: Validation of the Saharan dust plume conceptual model using lidar,
448 Meteosat, and ECMWF data, *Bull. Am. Meteorol. Soc.*, 80, 1045–1075, doi:10.1175/1520-
449 0477(1999)080<1045:VOTSDP>2.0.CO;2.

450 Kim, J., Akella, S., da Silva, A.M., Todling, R., McCarty, W.: Preliminary evaluation of influence of aerosols on the simulation
451 of brightness temperature in the NASA's Goddard Earth Observing System Atmospheric Data Assimilation System; Tech.
452 Rep. Ser. Glob. Model. Data Assim., Vol 49, TM-2018-104606, Goddard Space Flight Center, National Aeronautics and
453 Space Administration: Greenbelt, Maryland, US, 2018.

454 Kleist, D. T., Parrish, D. F., Derber, J. C., Treadon, R., Wu, W. S., and Lord, S.: Introduction of the GSI into the NCEP Global
455 Data Assimilation System. *Weather and Forecasting*, 24(6):16911705, 2009.

456 Letertre-Danczak, J.: The Use of Geostationary Radiance Observations at ECMWF and Aerosol Detection for Hyper-Spectral
457 Infrared Sounders: 1st and 2nd Years Report; EUMETSAT/ECMWF Fellowship Programme Research Reports, Vol 40,
458 European Centre for Medium Range Weather Forecasts: Shinfield Park, Reading, RG2 9AX, England, 2016.

459 Liu, Q. and Weng, F.: Advanced doubling-adding method for radiative transfer in planetary atmosphere, *J. Atmos. Sci.*, 63,
460 3459-3465, doi:10.1175/JAS3808.1, 2006.

461 Liu, Q., Han, Y., van Delst, P., and Weng, F.: Modeling aerosol radiance for NCEP data assimilation, in *Fourier Transform
462 Spectroscopy/Hyperspectral Imaging and Sounding of the Environment*, paper HThA5, OSA Technical Digest Series,
463 Optical Society of America, doi:10.1364/HISE.2007.HThA5, 2007.

464 Liu, Q. and Lu, C.-H.: Community Radiative Transfer Model for Air Quality Studies. In *Light Scattering Reviews*. 456
465 Kokhanovsky, A., Eds.; Springer Praxis Books, Springer-Verlag, Berlin – Heidelberg, Germany, Volume 457, pp. 67-115,
466 2016.

467 Liu, Z., Liu, Q., Lin, H.-C., Schwartz, C. S., Lee, Y.-H., and Wang, T.: Three-dimensional variational assimilation of MODIS
468 aerosol optical depth: Implementation and application to a dust storm over East Asia, *J. Geophys. Res.*, 116, D23206,
469 doi:10.1029/2011JD016159, 2011.

470 Lu, C.-H., da Silva, A., Wang, J., Moorthi, S., Chin, M., Colarco, P., Tang, Y., Bhattacharjee, P. S., Chen, S.-P., Chuang, H.-
471 Y., Juang, H.-M. H., McQueen, J., and Iredell, M.: The implementation of NEMS GFS Aerosol Component (NGAC)
472 version 1.0 for global dust forecasting at NOAA/NCEP, *Geosci. Model Dev.*, 9, 1905–1919, doi: 10.5194/gmd-9-1905-
473 2016, 2016.

474 Matricardi, M.: The inclusion of aerosols and clouds in RTIASI, the ECMWF fast radiative transfer model for the infrared
475 atmospheric sounding interferometer, *ECMWF Tech. Memo.*, 474, doi: 10.21957/1krvb28ql, 2005.

476 Merchant, C. J., Embury, O., Le Borgne, P. and Bellecm B.: Saharan dust in nighttime thermal imagery: Detection and
477 reduction of related biases in retrieved sea surface temperature, *Remote Sensing of Environ.*, 104, 15–30, doi:
478 10.1016/j.rse.2006.03.007, 2006.

479 Nalli, N. R., and L. L. Stowe, Aerosol correction for remotely sensed sea surface temperatures from the National Oceanic and
480 Atmospheric Administration advanced very high resolution radiometer, *J. Geophys. Res.*, 107(C10), 3172, doi:10.1029/
481 2001JC001162, 2002.

482 Pagowski, M., Liu, Z., Grell, G. A., Hu, M., Lin, H.-C., Schwartz, C. S., Implementation of aerosol assimilation in Gridpoint
483 Statistical Interpolation (v3.2) and WRF-Chem (v.3.4.1), *Geosci. Model Dev.*, 7, 1621–1627, doi:10.5194/gmd-7-1621-
484 2014, 2014.

485 Petty G: A First Course in Atmospheric Radiation, 2nd edition, Sundog Publishing, Madison, WI, 2006.

486 Peyridieu, S., Chdin, A., Tanr, D., Capelle, V., Pierangelo, C., Lamquin, N., and Armante, R.: Saharan dust infrared optical
487 depth and altitude retrieved from AIRS: a focus over North Atlantic comparison to MODIS and CALIPSO, *Atmos. Chem.*
488 *and Phys. Discuss.*, 9(5):2119921235, 2009.

489 Pierangelo, C., Chedin, A., Heilliette, S., Jacquinet-Husson, N., and R. Armante, R.: Dust altitude and infrared optical depth
490 from AIRS. *Atmos. Chem. Phys.*, 4, 1813-1822, doi: 10.5194/acp-4-1813-2004, 2004.

491 Randles, C. A., da Silva, A. M., Buchard, V., Colarco, P. R., Darmenov, A., Govindaraju, R., Smirnov, A., Holben, B., Ferrare,
492 R., Hair, J., Shinozuka, Y., Flynn, C., J: The MERRA-2 Aerosol Reanalysis, 1980 Onward. Part I: System Description and
493 Data Assimilation Evaluation, *Journal of Climate*, 30(17), 6823-6850, doi:10.1175/JCLI-D-16-0609.1, 2017.

494 Schwartz, C. S., Liu, Z., Lin, H.-C., and Cetola, J. D.: Assimilating aerosol observations with a “hybrid” variational-ensemble
495 data assimilation system, *J. Geophys. Res.-Atmos.*, 119, 4043–4069, doi:10.1002/2013JD020937, 2014.

496 Sokolik, I. N.: The spectral radiative signature of wind-blown mineral dust: Implications for remote sensing in the thermal IR
497 region: The spectral radiative signature of wind-blown mineral dust, *Geophys. Res. Lett.*, 29, 7-1-7-4,
498 doi:10.1029/2002GL015910, 2002.

499 Stegmann, P. G., Tang, G., Yang, P. and Johnson, B. T.: A stochastic model for density-dependent microwave Snow- and
500 Graupel scattering coefficients of the NOAA JCSDA community radiative transfer model, *J. Quant. Spec. Rad. Trans.*,
501 211, 9-24, doi:10.1016/j.jqsrt.2018.02.026, 2018.

502 Ukhov, A., Ahmadov, R., Grell, G., and Stenchikov, G.: Improving dust simulations in WRF-Chem model v4.1.3 coupled
503 with GOCART aerosol module, *Geosci. Model Dev. Disc.*, doi:10.5194/gmd-2020-92, 2021.

504 Wang, J., Bhattacharjee, P.S., Tallapragada, V., Lu, C.-H., Kondragunta, S., da Silva, A., Zhang, X., Chen, S.-P., Wei, S.-W.,
505 Darmenov, A.S., et al.: The implementation of NEMS GFS Aerosol Component (NGAC) Version 2.0 for global
506 multispecies forecasting at NOAA/NCEP – Part 1: Model descriptions., *Geosci. Model Dev.*, 11, 2315–2332,
507 doi:10.5194/gmd-11-2315-2018, 2018.

508 Weaver, C. J., Joiner, J., and Ginoux, P.: Mineral aerosol contamination of TIROS Operational Vertical Sounder (TOVS)
509 temperature and moisture retrievals., *J. Geophys. Res.*, 108, doi:10.1029/2002JD002571, 2003.

510 Wei, S.-W., Lu, C.-H., Liu, Q., Collard, A., Zhu, T., Grogan, D., Li, X., Wang, J., Grimbine, R., and Bhattacharjee, P.: The
511 impact of aerosols on satellite radiance data assimilation using NCEP global data assimilation system, *Atmos.*, 12(4), 432,
512 doi:10.3390/atmos12040432, 2021a.

513 Wei, S.-W., Lu, C.-H., Johnson, B. T., Dang, C., Stegmann, P., Grogan, D., Ge, G., and Hu, M.: The influence of aerosols on
514 satellite infrared radiance simulations and Jacobians: Numerical experiments of CRTM and GSI, *Remote. Sens.*, in review,
515 2021b.

516 Weng, F.: Advances in radiative transfer modeling in support of satellite data assimilation. *J. Atmos. Sci.*, 64, 3799–3807,
517 doi:10.1175/2007JAS2112.1, 2007.

518 Wu, W.-S., Purser, R. J., and Parrish, D. F.: Three-dimensional variational analysis with spatially inhomogeneous covariances,
519 *Mon. Weather Rev.*, 130, 2905–2916, doi:10.1175/1520-0493(2002)130<2905:TDVAWS>E2.0.CO;2, 2002.

520 Wu, M., Liu, X., Yu, H., Wang, H., Shi, Y., Yang, K., Darmenov, A., Wu, C., Wang, Z., Luo, T., Feng, Y., and Ke, Z.:
521 Understanding processes that control dust spatial distributions with global climate models and satellite observations,
522 *Atmos. Chem. Phys.*, 20, 13835–13855, <https://doi.org/10.5194/acp-20-13835-2020>, 2020.

523 Zhang L., Grell, G.A., Montuoro, R., McKeen, S. A., Bhattacharjee, P. S., Baker, B., Henderson, J., Pan, L., Frost, G. J.,
524 McQueen, J., Saylor, R., Ahmadov, R., Li, H., Wang, J., Stajner, I., Kondragunta, S., Zhang, X., Li, F.: Development of
525 GEFS-Aerosols into NOAAs Unified Forecast System UFS., *Geosci. Model Dev. Discuss.*, doi:10.5194/gmd-2021-378,
526 2021.